Generalized valence-force-field model of (Ga,In)(N,P) ternary alloys

Koushik Biswas, Alberto Franceschetti, and Stephan Lany
National Renewable Energy Laboratory, Golden, Colorado 80401, USA
(Received 17 June 2008; published 22 August 2008)

We present a generalized valence-force-field (VFF) model for the ternary III–V alloys (III=Ga, In and V=N, P) to predict the formation energies and atomic structures of ordered and disordered alloy configurations. For each alloy (GaInN, GaInP, GaNP, and InNP) the VFF parameters, which include bond-angle/bond-length interactions, are fitted to the first-principles calculated formation energies of 30 ternary structures. Compared to standard approaches where the VFF parameters are transferred from the individual binary III–V compounds, our generalized VFF approach predicts alloy formation energies and atomic structures with considerably improved accuracy. Using this generalized approach and random realizations in large supercells (4096 atoms), we determine the temperature-composition phase diagram, i.e., the binodal and spinodal decomposition curves, of the (Ga, In) (N, P) ternary alloys.

DOI: 10.1103/PhysRevB.78.085212 PACS number(s): 81.05.Ea, 61.66.Dk, 64.75.Qr

I. INTRODUCTION

Alloys of group-III nitride semiconductors (such as GaN and InN) and conventional III–V binary semiconductors (such as GaAs and InP) are being extensively studied for their potential applications in different fields. For example, the $Ga_{1-x}In_xN$ ternary (pseudobinary) alloy has widespread applications in blue-green light emitting diodes and other optoelectronic devices.[1,2] Recently, there have been attempts to use III–V ternary and quaternary alloys for photoelectrochemical water-splitting applications.[3,4] In this respect, such alloys offer several advantages over the III–V binaries. The band edges of III–V alloys can be tuned over a wide range of values to match the redox potentials for the water-splitting reactions. As an example, it has been shown that the band gap of GaN can be significantly reduced by alloying with other elements from groups III or V, e.g., In and P.[5–7] Furthermore, nitride alloys are relatively stable under photoelectrochemical operating conditions, which is not the case for other III–V semiconductor alloys.[4,8–11]

Accurate calculations of the formation energy and the phase diagram of III–V and III-N ternary and quaternary alloys often require the use of very large supercells that contain hundreds if not thousands of atoms. Such calculations are not feasible using standard first-principles methods. Therefore, the idea is to develop an energy functional that can be evaluated inexpensively and that can reliably predict the formation energies of large and/or complex structures. Many recent computational studies of III–V and III-N alloys have relied on the valence-force-field (VFF) method[12–15] or the cluster-expansion method.[16,17] In the VFF approach (originally developed by Keating[18] and later refined by Martin[19]), the ground-state atomic positions and lattice vectors are obtained by minimizing the strain energy, which is described by a set of bond-stretching and bond-bending parameters. The ground-state strain energy can then be used to compute the formation energy of ordered and disordered structures[20–27] as well as the phase diagram of ternary and quaternary alloys.[20–26,28–31] A major advantage of the VFF method over first-principles calculations is the relatively small computational cost required to relax large structures and calculate the formation energy of systems including thousands of atoms. At the same time, the VFF approach has the advantage over "discrete" methods such as the cluster expansion[32] of being able to accurately predict the atomic positions of lattice-mismatched semiconductor alloys and superlattices.[33,34]

The input parameters of the VFF energy functional are usually obtained from the experimentally measured (or theoretically calculated) elastic constants of the binary constituents[35–39] and are then used to calculate the formation energy of ternary and quaternary alloy systems.[20–24,28–31] In the original VFF scheme developed by Keating[18,19] [Keating valence force field (KVFF)], several constraints are imposed on the bond-bending parameter. For example, the bond-bending parameter is assumed to be identical for the cation or the anion-centered bonds (e.g., the bond-bending parameter for N-Ga-N equals that for Ga-N-Ga). In addition, a ternary or a quaternary alloy has mixed bonds, where three different atomic species form the bond configuration (e.g., Ga-N-In). In such cases, conventional KVFF defines the bond-bending parameter as the arithmetic average of the bond-bending parameters of the binary constituents that form the mixed bond (e.g., Ga-N-In is the "average" of Ga-N-Ga and In-N-In). As we will show below (see Sec. II and Table III), such parametrization of the KVFF functional often produces rather large deviations in the predicted alloy formation energies compared to density-functional calculations. In order to improve on this model, Silverman *et al.*[25,26] proposed an approach where these restrictions are lifted by the introduction of individual bond-bending parameters for the different atomic combinations. After fitting all VFF parameters to first-principles calculations of the formation energy of ordered structures, they found for the specific case of the $Ga_{1-x}In_xP$ alloy that the description of the alloy formation energies was improved over KVFF.

Using the VFF formulation without the restrictions of KVFF, and additionally considering the bond-angle/bond-length interaction parameters,[40] we have developed a generalized ternary valence-force-field (TVFF) model for the four ternary alloys in the (Ga, In) (N, P) zinc-blende system. For each ternary alloy, i.e., GaInN, GaInP, GaNP, and InNP, the TVFF parameters are obtained from a fit to the formation

TABLE I. LDA-calculated bulk modulus of the four binary compounds in the zinc-blende structure. Also shown are the VFF parameters α and β obtained directly from the LDA-calculated elastic constants C_{11} and C_{12} using Eq. (2) (column KVFF) and from a fit of α and β to C_{11}, C_{12}, and C_{44} (column KVFF-fit).

Binary compound	Bulk modulus (GPa)	VFF parameter	KVFF (N/m)	KVFF-fit (N/m)
GaN	200.8	α	84.63	85.75
		β	14.72	19.80
GaP	89.3	α	44.55	44.97
		β	10.74	11.68
InN	145.1	α	69.23	68.60
		β	7.30	11.26
InP	70.8	α	39.13	39.40
		β	6.36	7.57

energies of an extensive set of *ternary* ordered and disordered structures—calculated using density-functional theory (DFT) in the local-density approximation (LDA). In contrast to the KVFF model, where the VFF parameters are defined only from the properties of the *binary* constituents, our model of the TVFF energy functional is "trained" to evaluate ternary structures and considerably improves the description of the formation energies for all four ternary alloys. The reliability of the fitted parameters is further validated against LDA-calculated formation energies and atomic positions of several test structures that were not originally included in the fit. Using this generalized TVFF model, we predict (Sec. III) the formation energies and temperature-composition phase diagrams of the $Ga_{1-x}In_xN$, $Ga_{1-x}In_xP$, $GaN_{1-x}P_x$, and $InN_{1-x}P_x$ random alloys.

II. COMPUTATIONAL METHODS

A. First-principles calculations

First-principles LDA calculations were performed to fit the parameters of the TVFF energy functional and to test the predictions of TVFF calculations. We have used the projector augmented wave method[41] as implemented in the Vienna *ab initio* simulation package.[42]

The compounds considered here are GaN, GaP, InN, and InP in the zinc-blende lattice structure as well as several ordered and disordered (Ga, In) (N, P) ternary structures. The Ga $3d$ and In $4d$ orbitals were treated as valence states in all the calculations. We performed convergence tests with respect to the energy cutoff and the k-point sampling. We found that a plane-wave energy cutoff of 520 eV is sufficient to calculate the structural properties with good accuracy and it was used in all the calculations. Brillouin-zone integrations were performed using Γ-centered k-point meshes that are equivalent[43] to the $6\times6\times6$ Monkhorst-Pack k-point grid for an eight atom cubic unit cell.[44] All total energies were converged to within 2 meV/cation or less.

B. Valence-force-field calculations

According to the KVFF model of tetrahedral semiconductors, the strain energy can be written as[18,19]

$$U_{\mathrm{KVFF}} = \sum_{i=1}^{N}\left(\sum_{j=1}^{4}\left\{\frac{3}{8d_{ij}^2}\alpha_{ij}(\vec{r}_{ij}\cdot\vec{r}_{ij}-d_{ij}^2)^2 + \sum_{k=1,k\neq j}^{4}\frac{3}{8d_{ij}d_{ik}}\beta_{ijk}[\vec{r}_{ij}\cdot\vec{r}_{ik}-d_{ij}d_{ik}\cos(\Theta_{ijk})]^2\right\}\right), \tag{1}$$

where α_{ij} and β_{ijk} are the bond-stretching and bond-bending parameters, respectively, r_{ij} is the nearest-neighbor distance, d_{ij} is the ideal bond length, and θ_{ijk}^0 is the ideal unrelaxed tetrahedral bond angle (109.5°). For a given atom i, the indices j and k run over the four nearest-neighbor atoms. In the KVFF model, the parameters α and β are derived from the elastic constants C_{11} and C_{12} of the binary compound. C_{11} and C_{12} can be either measured or calculated from first principles. The KVFF parameters α and β can be obtained by inverting the following equations:[18]

$$C_{11}+2C_{12}=\frac{\sqrt{3}}{4d}(3\alpha+\beta),$$

$$C_{11}-C_{12}=\frac{\sqrt{3}}{d}\beta. \tag{2}$$

Alternatively, one can fit the two VFF parameters α and β to the measured or calculated values of all the three zinc-blende elastic constants C_{11}, C_{12}, and C_{44}. As shown in a study by Grosse and Neugebauer,[27] this approach improves the calculated VFF formation energies of GaInN alloys. Table I shows the calculated LDA values of the bulk modulus of the four binary semiconductors considered here, along with the KVFF parameters α and β obtained from Eq. (2) (column "KVFF"), and those obtained by the fit of all three elastic constants (column "KVFF-fit"). These KVFF parameters are used below for comparison with our generalized TVFF model.

C. Generalized TVFF energy functional

1. Definition of the TVFF functional

As mentioned in Sec. I, the motivation for the TVFF formulation is to lift the restrictions present in the conventional

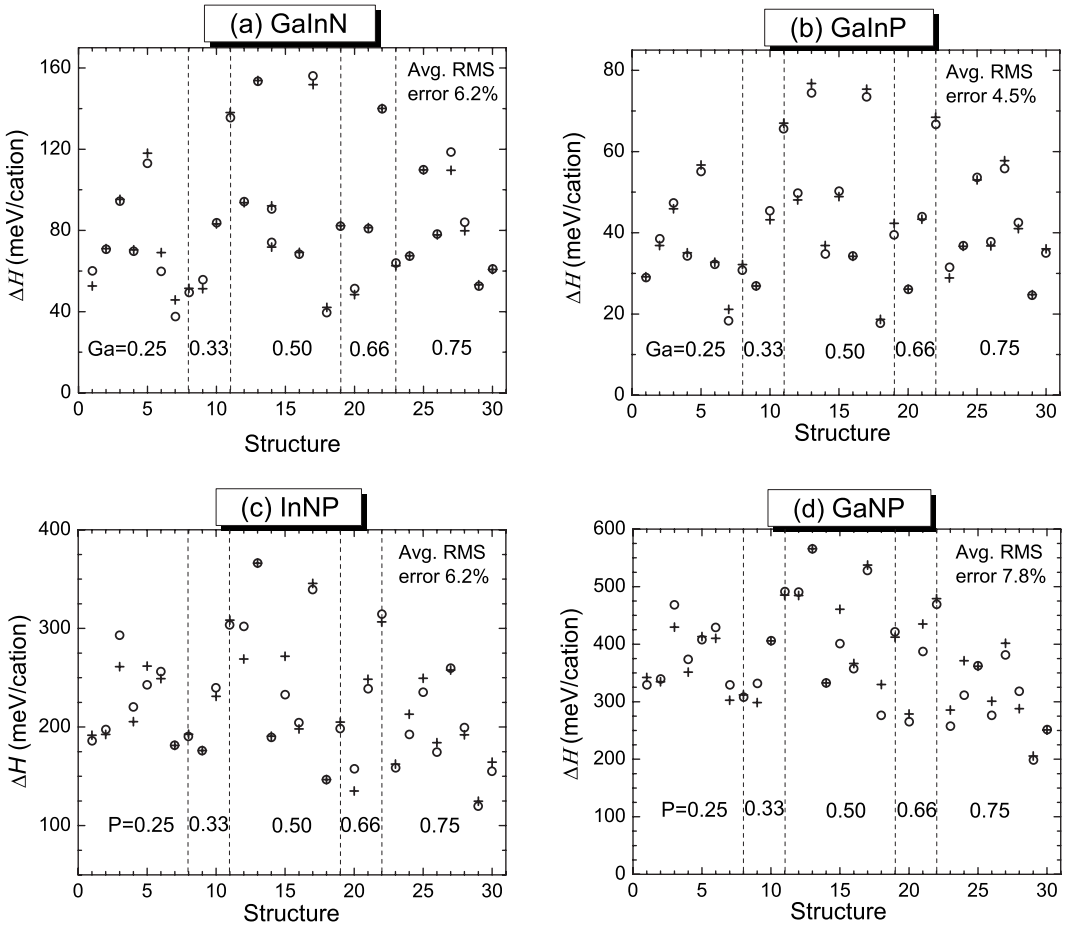

FIG. 1. Calculated mixing enthalpies ΔH of 30 different structures (27 ordered +3 pseudorandom) at different cation/anion concentrations of the (a) GaInN, (b) GaInP, (c) InNP, and (d) GaNP alloys. The circles denote LDA results while the crosses denote TVFF results. The TVFF parameters were fitted to the LDA-calculated mixing enthalpies. The relative rms errors of the fitted energies with respect to LDA averaged over all structures are also shown.

KVFF model. First, in the KVFF model the bond-bending parameter β is assumed to be the same for cation-centered and anion-centered bonds. For example, in the common-anion alloy $A_{1-x}B_xC$, KVFF assumes $\beta_{ACA}=\beta_{CAC}$ and $\beta_{BCB}=\beta_{CBC}$. Second, in the KVFF model the mixed-bond parameter β_{ACB} is chosen as the arithmetic average of the binary constituents, i.e., $\beta_{ACB}=1/2(\beta_{ACA}+\beta_{BCB})$. Besides removing these restrictions and treating all β_{ijk} as free parameters without constraints, we use for our TVFF model an extended version of the KVFF energy functional (originally proposed by Kim *et al.*)[40] in which a bond-angle/bond-length interaction parameter σ_{ijk} is introduced,

$$U_{\mathrm{TVFF}} = \sum_{i=1}^{N}\left(\sum_{j=1}^{4}\left\{\frac{3}{8d_{ij}^2}\alpha_{ij}(\vec{r}_{ij}\cdot\vec{r}_{ij}-d_{ij}^2)^2 + \sum_{k=1,k\neq j}^{4}\frac{3}{8d_{ij}d_{ik}}\beta_{ijk}[\vec{r}_{ij}\cdot\vec{r}_{ik}-d_{ij}d_{ik}\cos(\theta_{ijk}^0)]^2\right\}\right) + \sum_{i=1}^{N}\sum_{j=1}^{4}\left[\sum_{k=1,k\neq j}^{4}\frac{3}{d_{ij}d_{ik}}\sigma_{ijk}(\vec{r}_{ij}\cdot\vec{r}_{ij}-d_{ij}^2) \times(\vec{r}_{ij}\cdot\vec{r}_{ik}-d_{ij}d_{ik}\cos\theta_{ijk}^0)\right]. \quad (3)$$

For the ternary systems $A_{1-x}B_xC$, we parameterize β and σ as follows:

$$\beta_{ACA}=\bar{\beta}_{AC}+\Delta\beta_{AC},$$

$$\beta_{CAC}=\bar{\beta}_{AC}-\Delta\beta_{AC},$$

$$\beta_{BCB}=\bar{\beta}_{BC}+\Delta\beta_{BC},$$

$$\beta_{CBC}=\bar{\beta}_{BC}-\Delta\beta_{BC},$$

$$\sigma_{ACA}=\bar{\sigma}_{AC}+\Delta\sigma_{AC},$$

$$\sigma_{CAC}=\bar{\sigma}_{AC}-\Delta\sigma_{AC},$$

$$\sigma_{BCB}=\bar{\sigma}_{BC}+\Delta\sigma_{BC},$$

TABLE II. Fitted TVFF parameters for the GaInN, GaInP, InNP, and GaNP ternary alloys.

Ternary alloy	Fitted TVFF parameters α (N/m)	β (N/m)	σ (N/m)
GaInN	$\alpha_{GaN}=114.0$	$\bar{\beta}_{GaN}=10.9$; $\Delta\beta_{GaN}=1.5$	$\bar{\sigma}_{GaN}=-17.3$; $\Delta\sigma_{GaN}=-15.4$
	$\alpha_{InN}=50.9$	$\bar{\beta}_{InN}=10.7$; $\Delta\beta_{InN}=1.0$	$\bar{\sigma}_{InN}=-16.2$; $\Delta\sigma_{InN}=-17.8$
		$\beta_{GaInN}=14.8$	$\sigma_{GaInN}=-35.4$
GaInP	$\alpha_{GaP}=31.6$	$\bar{\beta}_{GaP}=8.8$; $\Delta\beta_{GaP}=8.1$	$\bar{\sigma}_{GaP}=-3.2$; $\Delta\sigma_{GaP}=-9.3$
	$\alpha_{InP}=49.6$	$\bar{\beta}_{InP}=7.1$; $\Delta\beta_{InP}=3.3$	$\bar{\sigma}_{InP}=-4.2$; $\Delta\sigma_{InP}=1.8$
		$\beta_{GaInP}=6.2$	$\sigma_{GaInP}=2.6$
InNP	$\alpha_{InN}=65.2$	$\bar{\beta}_{InN}=17.1$; $\Delta\beta_{InN}=0.5$	$\bar{\sigma}_{InN}=-7.3$; $\Delta\sigma_{InN}=-12.2$
	$\alpha_{InP}=11.7$	$\bar{\beta}_{InP}=11.3$; $\Delta\beta_{InP}=-10.5$	$\bar{\sigma}_{InP}=-3.0$; $\Delta\sigma_{InP}=7.1$
		$\beta_{InNP}=24.3$	$\sigma_{InNP}=-2.4$
GaNP	$\alpha_{GaN}=18.8$	$\bar{\beta}_{GaN}=33.6$; $\Delta\beta_{GaN}=1.2$	$\bar{\sigma}_{GaN}=-6.2$; $\Delta\sigma_{GaN}=-15.6$
	$\alpha_{GaP}=90.6$	$\bar{\beta}_{GaP}=15.5$; $\Delta\beta_{GaP}=0.5$	$\bar{\sigma}_{GaP}=-6.9$; $\Delta\sigma_{GaP}=-22.6$
		$\beta_{GaNP}=10.6$	$\sigma_{GaNP}=-12.4$

$$\sigma_{CBC}=\bar{\sigma}_{BC}-\Delta\sigma_{BC}, \tag{4}$$

$$\Delta H(A_{1-x}B_xC)=E(A_{1-x}B_xC)-xE(BC)-(1-x)E(AC), \tag{5}$$

where $\bar{\beta}$, $\Delta\beta$, $\bar{\sigma}$, and $\Delta\sigma$ are fitting parameters. Also, we include β_{ACB} and σ_{ACB} as free fitting parameters for the mixed bonds. Therefore, for each ternary system $A_xB_{1-x}C$, we have two bond-stretching parameters (α_{AC} and α_{BC}), five bond-bending parameters ($\bar{\beta}_{AC}$, $\bar{\beta}_{BC}$, $\Delta\beta_{AC}$, $\Delta\beta_{BC}$, and β_{ACB}), and five bond-angle/bond-length parameters ($\bar{\sigma}_{AC}$, $\bar{\sigma}_{BC}$, $\Delta\sigma_{AC}$, $\Delta\sigma_{BC}$, and σ_{ACB}) for a total of twelve fitting parameters.

2. Fit of the TVFF parameters

In the conventional KVFF approach, the VFF parameters are determined for the pure binary compounds and are then transferred to the ternary alloy system by applying the above described constraints. Besides the removal of these constraints, the determination of the TVFF parameters relies on input from first-principles data of actual ternary alloy structures. Thus, the TVFF parameters are constructed on the basis of the same alloy system that is to be described by TVFF, without relying on the assumption of transferability from the binary compounds to the ternary alloy. Specifically, the VFF parameters of Eq. (3) are fitted to the LDA-calculated formation energies of 27 ordered structures and three "pseudorandom" structures for each ternary alloy (GaInN, GaInP, GaNP, and InNP). The 27 ordered structures include all the possible zinc-blende structures with up to eight atoms (four anions and four cations) in the unit cell. The term pseudorandom is used to describe 64-atom unit cells where the cations and anions are randomly distributed in their respective sublattices. Each of the 30 different structures is fully relaxed (both in LDA and in VFF) by optimizing the cell-external and cell-internal degrees of freedom. At the relaxed geometry, the alloy mixing enthalpy ΔH is calculated as

where $E(A_{1-x}B_xC)$ is the total energy of the ternary structure of composition x and $E(AC)$ and $E(BC)$ are the total energies of the two binary constituents.

The initial values of the TVFF parameters of Eq. (3) were obtained by fitting to the LDA-calculated elastic constants of the four binary compounds. The TVFF parameters were then allowed to change until the best least-squares fit of the TVFF formation energies to the LDA formation energies was achieved. Figure 1 shows the results of the fit for the four ternary systems considered here, along with the average root-mean-square (rms) fit error for each ternary. The fitted TVFF parameters for the four ternary alloys are summarized in Table II.

3. Predictive ability of TVFF

To evaluate the ability of the TVFF functional to predict the properties of new structures, we consider a set of test structures that were not included in the fit. For each of the four ternaries, we consider three 32-atom special quasirandom structures (SQSs)[45,46] at $x=0.25$, 0.50, and 0.75 and the Q8 and Q16 structures at $x=0.25$ and 0.75. The Q8 is a 16 atom per cell layered structure along the $\langle 201\rangle$ direction.[47] The Q16 structure has a 32-atom tetragonal unit cell.[48] The rms deviation of ΔH for the different methods with respect to LDA is calculated as $\delta=\sqrt{(1/n)\Sigma|\Delta H_{LDA}-\Delta H_{VFF}|^2}$, where n is the total number of test structures for each ternary and VFF=TVFF, KVFF, or KVFF-fit. Table III shows the calculated values of ΔH from LDA, KVFF, KVFF-fit, and TVFF for all the test structures as well as the calculated values of δ. We should point out that in the case of the highly lattice-mismatched InNP and GaNP alloys, KVFF-fit generally gives a better agreement with LDA than KVFF. However,

TABLE III. Mixing enthalpies ΔH obtained from LDA, TVFF, KVFF, and KVFF-fit for different test structures of the four ternary alloys at the compositions $x=0.25$, $x=0.50$, and $x=0.75$. For the different VFF models, δ gives the rms deviation relative to ΔH in LDA. The last column gives the rms of the relative difference in the nearest-neighbor distances between LDA and TVFF.

Chemical composition	Structure	ΔH_{LDA} (meV/cation)	ΔH_{TVFF} (meV/cation)	ΔH_{KVFF} (meV/cation)	$\Delta H_{\mathrm{KVFF\text{-}fit}}$ (meV/cation)	Δd_{nn} (%)
$Ga_{0.25}In_{0.75}N$	32-atom SQS	54.2	54.4	50.6	67.9	0.5
	Q8	36.1	39.8	33.6	47.4	0.4
	Q16	37.6	39.9	34.6	48.4	0.4
$Ga_{0.50}In_{0.50}N$	32-atom SQS	91.9	88.4	79.9	101.8	0.6
$Ga_{0.75}In_{0.25}N$	32-atom SQS	64.9	65.3	58.4	73.6	0.5
	Q8	40.9	42.9	46.7	60.3	0.7
	Q16	41.3	43.4	46.4	59.9	0.7
RMS deviation, δ			2.4	6.3	13.8	
$Ga_{0.25}In_{0.75}P$	32-atom SQS	25.8	27.0	31.2	34.6	0.1
	Q8	16.3	18.6	22.1	25.0	0.2
	Q16	16.6	19.0	22.5	25.4	0.1
$Ga_{0.50}In_{0.50}P$	32-atom SQS	43.5	44.7	50.8	62.5	0.2
$Ga_{0.75}In_{0.25}P$	32-atom SQS	29.8	32.2	34.0	36.7	0.1
	Q8	18.6	19.4	27.7	29.9	0.1
	Q16	18.3	19.3	27.5	29.9	0.1
RMS deviation, δ			1.7	6.9	11.3	
$InN_{0.25}P_{0.75}$	32-atom SQS	146.4	168.7	125.3	151.9	0.6
	Q8	103.2	107.1	85.1	103.9	0.5
	Q16	104.1	109.2	86.9	106.2	0.4
$InN_{0.50}P_{0.50}$	32-atom SQS	240.6	256.9	176.7	218.5	0.6
$InN_{0.75}P_{0.25}$	32-atom SQS	170.0	178.0	116.5	150.2	1.3
	Q8	139.8	156.8	91.2	122.9	0.8
	Q16	140.9	156.7	91.4	122.4	0.7
RMS deviation, δ			14.2	42.8	14.8	
$GaN_{0.25}P_{0.75}$	32-atom SQS	250.3	268.1	220.9	247.4	0.4
	Q8	177.7	188.9	154.4	172.5	0.5
	Q16	179.1	191.2	156.9	175.9	0.5
$GaN_{0.50}P_{0.50}$	32-atom SQS	402.9	413.5	308.2	350.1	1.0
$GaN_{0.75}P_{0.25}$	32-atom SQS	303.8	323.4	208.5	242.0	1.1
	Q8	272.7	273.6	173.3	207.8	0.7
	Q16	274.7	270.9	172.7	206.5	0.7
RMS deviation, δ			12.5	75.8	47.1	

our TVFF results consistently show a better agreement with LDA, compared to KVFF and KVFF-fit for all ternary alloys.

Recently, Chen *et al.*[49] showed that the KVFF model predicts the famatinite (FM) structure [a $(AC)_3/(BC)_1$ superlattice structure oriented along the $\langle 201 \rangle$ direction][50] as the lowest energy structure for the $Ga_{0.25}In_{0.75}N$ and $GaN_{0.25}P_{0.75}$ alloys whereas in the direct DFT calculations in the generalized gradient approximation (GGA), either the Q8 or the Q16 structure was lower in energy than FM for all ternary (Ga, In) (N, P) alloys at the $x=0.25$ and 0.75 compositions. Unlike other VFF models,[49,51] our TVFF model agrees with the direct DFT calculation (GGA in Ref. 49 and LDA in the present work) that FM is not the lowest energy structure within the (Ga, In) (N, P) alloy system.

As a second test of the TVFF energy functional, we compare the TVFF relaxed atomic positions of the structures of Table III with those predicted by LDA. The rms of the relative difference in the nearest-neighbor distances between LDA and TVFF can be calculated as

$$\Delta d_{nn} = \sqrt{\frac{1}{4N}\sum_{i=1}^{N}\sum_{j=1}^{4}\left(\frac{d_{ij}^{\mathrm{LDA}} - d_{ij}^{\mathrm{TVFF}}}{d_{ij}^{\mathrm{LDA}}}\right)^2}, \quad (6)$$

where d_{ij}^{LDA} and d_{ij}^{TVFF} are the nearest-neighbor distances in LDA and TVFF, respectively. N is the total number of atoms in the supercell. The calculated values of Δd_{nn} are shown in Table III for all the test structures considered here. In all cases, we find that the final relaxed structures from TVFF do not deviate much from that of LDA (1.3% being the largest deviation). In most cases, the agreement of the atomic positions and the nearest-neighbor distances obtained from TVFF and LDA were within 1%, which is comparable to the accuracy of the LDA calculations (the LDA calculated lattice constant is typically underestimated by 1% relative to experiment).

III. THERMODYNAMIC PROPERTIES OF $Ga_{1-x}In_xN$, $Ga_{1-x}In_xP$, $GaN_{1-x}P_x$, and $InN_{1-x}P_x$ ALLOYS USING TVFF

A. Mixing enthalpies (ΔH) of random alloys

In order to have an accurate representation of the disordered alloy, we used a large 4096-atom supercell and calculated the formation energy as the average over ten different random realizations at each composition. The small spread of ΔH among the different realizations (<2meV/cation, see Ref. 52) illustrates that finite-size effects are sufficiently converged at this cell size. The ΔH as a function of composition x is represented by a third-order polynomial. The functional form and the values of the coefficients are given in Table IV. Figure 2 shows the TVFF predicted ΔH of the random $Ga_{1-x}In_xN$, $Ga_{1-x}In_xP$, $GaN_{1-x}P_x$, and $InN_{1-x}P_x$ ternary alloys as a function of the composition. For comparison, Fig. 2 also shows the ΔH of the ordered structures used in the fit of the

TABLE IV. Values of the coefficients a and b in the polynomial that represents ΔH as a function of composition x: $\Delta H(x) = (a - bx)x(1-x)$.

Ternary alloy	a	b
GaInN	371.3	76.7
GaInP	178.8	27.2
InNP	1021.0	173.2
GaNP	2003.0	834.3

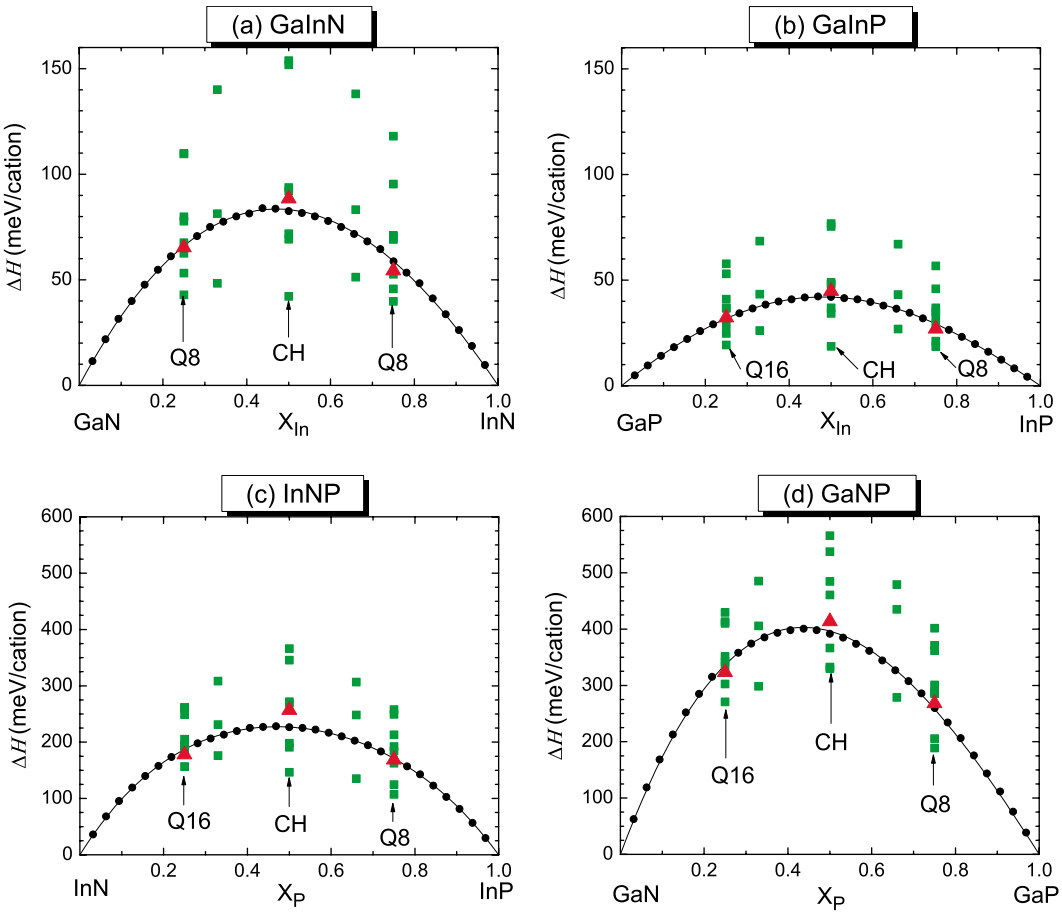

FIG. 2. (Color online) Average TVFF mixing enthalpy ΔH (solid curve and symbols) of (a) GaInN, (b) GaInP, (c) InNP, and (d) GaNP zinc-blende random alloys calculated using a 4096-atom supercell and ten random realizations at each composition. Also shown are the calculated energies of ordered structures (solid squares) and 32-atom SQSs (solid triangles) at different compositions—all were obtained using TVFF. Some of the lowest energy ordered structures, e.g., Q8/Q16 at compositions x=0.25 and 0.75 and chalcopyrite (CH) at x =0.50 are identified by arrows.

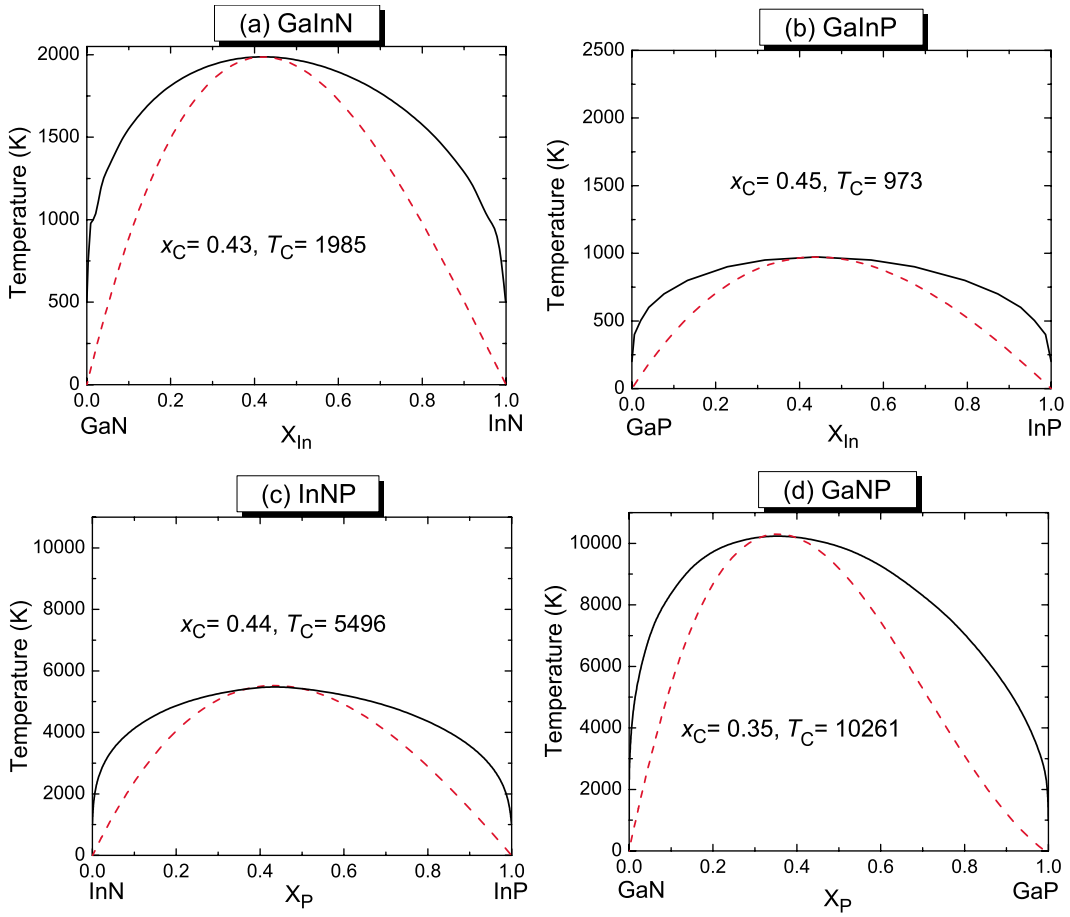

FIG. 3. (Color online) Predicted temperature-composition phase diagram of (a) GaInN, (b) GaInP, (c) InNP, and (d) GaNP zinc-blende random alloys. The solid and dashed curves correspond to the binodal and spinodal decomposition lines, respectively. The consolute temperature (T_C) and the corresponding alloy compositions (x_C) are also shown.

TVFF parameters as well as that of the 32-atom SQS test structures listed in Table III. Note that the mixing enthalpies of the highly lattice-mismatched mixed-anion alloys (III-$N_{1-x}P_x$) are much larger than those of the mixed-cation alloys ($Ga_{1-x}In_x$-V). The ΔH of all four alloys is found to be asymmetric and skewed toward the Ga-rich side in the $Ga_{1-x}In_x$-V and toward the N-rich side in the III-$N_{1-x}P_x$ alloys.

It is worth mentioning that in some cases, the mixing enthalpies of the SQS structures somewhat deviate from those of the random alloys calculated using a 4096-atom supercell (see Fig. 2). For example, the mixing enthalpy of the $InN_{0.5}P_{0.5}$ alloy calculated using the 4096-atom cell is 226.3 meV/cation while the mixing enthalpy of the 32-atom SQS structure at the same composition is 256.9 meV/cation (note that the SQS and supercell energies in Fig. 2 are both calculated with the TVFF functional and that the SQS energies predicted by TVFF agree very well with the direct LDA calculation as shown in Table III). Furthermore, a random-alloy model based exclusively on SQS structures would predict a different asymmetry of the mixing enthalpy with respect to composition (see Fig. 2). For example, in $GaN_{1-x}P_x$ the SQS structures predict a less pronounced asymmetry (about 4.5%) than that of the supercell method (about 6.3%)—all relative to the regular solution model which would give a symmetric ΔH.

Since GaInN is by far the most investigated[17,20,22–24,29,39,53–58] case among the III–V ternary alloys, we now compare our results with a few recent theoretical works on this alloy system. Compared to previous KVFF calculations,[20,22,23] our generalized TVFF model gives somewhat larger energies with the maximum mixing enthalpy ΔH_{max}=83.7 meV/cation (being up to ~20 meV/cation larger than the prior results). Compared to the first-principles results based on the SQS model of the random alloy in Ref. 53, our ΔH_{max} is smaller by about 30 meV/cation. This difference is due to different numerical results for the ΔH of the SQS in LDA (see Table III) and, therefore, it is not related to the TVFF model employed in the present work. Similar mixing enthalpies to those reported in the present work were obtained by Purton *et al.*[54] using interatomic potentials and by Liu *et al.* [see Fig. 3(a) in Ref. 17] using the cluster-expansion method. For the GaInP alloy, our calculated mixing enthalpies (ΔH_{max} =42.3 meV/cation) are similar to those obtained by Silverman *et al.*[25] with a similar methodology. For the mixed-anion GaNP and InNP alloys, few theoretical estimates of the mixing enthalpy are available. Notably, in the case of GaNP our calculated ΔH_{max}=403.5 meV/cation is larger than the value $\Delta H_{max} \approx 300$ meV/cation obtained by Ho and Stringfellow[21] using KVFF within the regular solution model (no asymmetry). Again, based on the regular solution model,

Takayama *et al.*[24] reported a $\Delta H_{\max} \approx 355$ and 190 meV/cation for wurtzite GaNP and InNP, respectively, which are also lower than the present results (our $\Delta H_{\max}$ for InNP is 228.1 meV/cation).

B. Phase diagrams

Having determined the alloy mixing enthalpies $\Delta H(x)$ of the four (Ga, In) (N, P) ternary alloys for a realistic random-alloy model, we now discuss the temperature versus composition (T-x) phase diagrams for the four alloys. The Gibbs free energy of mixing of an alloy of composition x is

$$(\Delta Gx) = \Delta H(x) - T\Delta S(x), \tag{7}$$

where we take the entropy of mixing (ΔS) as the configurational entropy of the ideal random alloy,

$$\Delta S(x) = -k_B[x \ln x + (1-x)\ln(1-x)]. \tag{8}$$

According to general alloy theory,[59] the binodal curve (equilibrium miscibility) is constructed from the $\Delta G(x)$ graph using a common tangent approach and the spinodal curve is determined from the inflection points ($\partial^2 \Delta G / \partial x^2 = 0$) at a given temperature. For the purpose of the present work, we do not include short-range ordering or vibrational effects in the phase-diagram calculation. Those effects generally lead to moderate quantitative corrections in the phase-diagram calculation.[16,25,53] Rather, we focus here on the effect of the alloy mixing enthalpies, which (in the present work) are based on consistent data sets of first-principles calculated formation energies for the four different alloy systems and are obtained with a realistic model of the random alloys via the generalized TVFF functional.

The calculated (T-x) phase diagrams are shown in Fig. 3—also indicating the consolute temperatures (T_C) and the corresponding alloy compositions (x_C). The existence of a miscibility gap indicates that spinodal decomposition should occur. For example, we predict a miscibility gap between $x=0.11$ and $x=0.79$ in the $Ga_{1-x}In_xN$ alloy at 1000 K, in agreement with recent phase diagram calculations.[17,53,54] Indeed, many experimental studies have found signatures of phase separation or spinodal decomposition.[60–65] Also, spinodal decomposition is expected to promote periodic compositional modulation as observed by transmission electron microscopy.[66] Note however that the tendency toward spinodal decomposition and phase separation depends delicately on the presence of strain in case of epitaxial growth (not considered here), which can lead to negative formation energies and, hence, to the suppression of the miscibility gap.[17]

The calculated phase diagrams are significantly asymmetric with respect to composition for all four alloys—resulting from the asymmetric behavior of $\Delta H(x)$ (see Fig. 2)—whereas such asymmetries are neglected in regular solution models. The use of a realistic model of the random alloy is essential to reliably predict asymmetries in the phase diagram. The largest asymmetry is found in the $GaN_{1-x}P_x$ alloy, indicating that N substitution in GaP requires considerably less energy than P substitution in GaN (see Fig. 2).

The T_C in the mixed-anion alloys III-$N_{1-x}P_x$ are much larger compared to the mixed-cation alloys $Ga_{1-x}In_x$-V due to the larger lattice mismatch (Fig. 3). Indeed, the calculated equilibrium solubility in the dilute nitride alloys is generally very low—far less than 1% (Refs. 21 and 67) (from our calculated formation energies, we obtain an equilibrium solubility of only, e.g., $c_{\mathrm{sol}} = 3.5 \times 10^{16}$ cm^{-3} for N in GaP at $T = 1000$ K). The fact that III–V alloys with higher N concentrations (up to a few per cent) can actually be grown has previously been attributed to nonequilibrium growth,[68] to surface-reconstruction-enhanced solubility,[67] or to the effect of epitaxial strain.[69] However, we find that due to the asymmetric phase-diagram (Fig. 3), dilute GaP:N alloy remains remarkably stable against spinodal decomposition despite the very low-N equilibrium solubility. Thus, once a sufficiently high concentration of N atoms is incorporated (e.g., using nonequilibrium growth methods), it remains metastable (e.g., up to 8.6% N content at $T=1000$ K) before the onset of the two-phase spinodal decomposition (see Fig. 3). In contrast, dilute P doping in GaN is limited to only 1.6% at this temperature (see Fig. 3). Irrespective of the low-equilibrium solubility, the relative stability against spinodal decomposition in case of N alloying into GaP is an important prerequisite for the prospective application of GaNP alloys for photoelectrochemical water splitting, where it has been shown that N incorporation in III–V alloys enhance their resistance toward photocorrosion in the electrolyte solution.[4]

IV. CONCLUSIONS

We have developed a generalized VFF model for the ternary GaInN, GaInP, GaNP, and InNP alloys, which is based on first-principles calculated formation energies of ordered alloy structures. The TVFF functional is able to predict the formation energy of new structures (not included in the fit of the TVFF parameters) with much better accuracy than the standard VFF approaches and yield atomic structures very close to the first-principles calculations. Using the TVFF functional, we have calculated the temperature-composition phase diagrams (i.e., the binodal and spinodal decomposition curves) of the $Ga_{1-x}In_xN$, $Ga_{1-x}In_xP$, $GaN_{1-x}P_x$, and $InN_{1-x}P_x$ alloys in the zinc-blende lattice structure. In the case of GaNP dilute nitride alloys, which are presently considered for application as photoelectrochemical water-splitting materials, the pronounced asymmetry in the phase diagram indicates relative stability of N doping against spinodal decomposition despite the very high-consolute temperature above 10 000 K.

ACKNOWLEDGMENTS

We thank Mayeul d'Avezac (National Renewable Energy Laboratory) for the use of the valence-force-field code and for helpful discussions. This work was funded by the Office of Energy Efficiency and Renewable Energy, U.S. Department of Energy under Contract No. DE-AC36-99GO10337 to NREL through NREL's Laboratory Directed Research and Development program.

[1] S. Nakamura, M. Senoh, N. Iwasa, and S. Nagahama, Jpn. J. Appl. Phys., Part 2 **34**, L797 (1995).
[2] S. Nakamura, M. Senoh, S. Nagahama, N. Iwasa, T. Yamada, T. Matsushita, H. Kiyoko, and Y. Sugimoto, Jpn. J. Appl. Phys., Part 2 **35**, L74 (1996).
[3] T. Bak, J. Nowotny, M. Rekas, and C. C. Sorrell, Int. J. Hydrogen Energy **27**, 991 (2002), and references therein.
[4] T. G. Deutsch, C. A. Koval, and J. A. Turner, J. Phys. Chem. B **110**, 25297 (2006).
[5] L. Bellaiche, S.-H. Wei, and A. Zunger, Phys. Rev. B **56**, 10233 (1997).
[6] L. Bellaiche, T. Mattila, L.-W. Wang, S.-H. Wei, and A. Zunger, Appl. Phys. Lett. **74**, 1842 (1999).
[7] K. Iwata, H. Asahi, K. Asami, and S. Gonda, J. Cryst. Growth **175-176**, 150 (1997).
[8] J. R. Mileham, S. J. Pearton, C. R. Abernathy, J. D. MacKenzie, R. J. Shul, and S. P. Kilcoyne, J. Vac. Sci. Technol. A **14**, 836 (1996).
[9] M. S. Minsky, M. White, and E. L. Hu, Appl. Phys. Lett. **68**, 1531 (1996).
[10] K. Maeda, T. Takata, M. Hara, N. Saito, Y. Inoue, H. Kobayashi, and K. Domen, J. Am. Chem. Soc. **127**, 8286 (2005).
[11] J. D. Beach, R. T. Collins, and J. A. Turner, J. Electrochem. Soc. **150**, A899 (2003).
[12] L. Bellaiche, S.-H. Wei, and A. Zunger, Phys. Rev. B **56**, 13872 (1997).
[13] T. Mattila and A. Zunger, J. Appl. Phys. **85**, 160 (1999).
[14] Y. Zhang, A. Mascarenhas, and L. W. Wang, Phys. Rev. B **64**, 125207 (2001).
[15] O. Rubel, K. Volz, T. Torunski, S. D. Baranovskii, F. Grosse, and W. Stolz, Appl. Phys. Lett. **85**, 5908 (2004).
[16] B. P. Burton, A. van de Walle, and U. Kattner, J. Appl. Phys. **100**, 113528 (2006).
[17] J. Z. Liu and A. Zunger, Phys. Rev. B **77**, 205201 (2008).
[18] P. N. Keating, Phys. Rev. **145**, 637 (1966).
[19] R. M. Martin, Phys. Rev. B **1**, 4005 (1970).
[20] I. Ho and G. B. Stringfellow, Appl. Phys. Lett. **69**, 2701 (1996).
[21] I. Ho and G. B. Stringfellow, J. Cryst. Growth **178**, 1 (1997).
[22] T. Saito and Y. Arakawa, Phys. Rev. B **60**, 1701 (1999).
[23] T. Takayama, M. Yuri, K. Itoh, T. Baba, and J. S. Harris, Jr., J. Appl. Phys. **88**, 1104 (2000).
[24] T. Takayama, M. Yuri, K. Itoh, and J. S. Harris, Jr., J. Appl. Phys. **90**, 2358 (2001).
[25] A. Silverman, A. Zunger, R. Kalish, and J. Adler, Phys. Rev. B **51**, 10795 (1995).
[26] A. Silverman, A. Zunger, R. Kalish, and J. Adler, J. Phys.: Condens. Matter **7**, 1167 (1995).
[27] F. Grosse and J. Neugebauer, Phys. Rev. B **63**, 085207 (2001).
[28] R. Asomoza, V. A. Elyukhin, and R. Peña-Sierra, Appl. Phys. Lett. **78**, 2494 (2001).
[29] J. Adhikari and D. A. Kofke, J. Appl. Phys. **95**, 4500 (2004).
[30] R. Asomoza, V. A. Elyukhin, and R. Peña-Sierra, Appl. Phys. Lett. **81**, 1785 (2002).
[31] V. A. Elyukhin, L. P. Sorokina, and M. Rodriguez de Santiago, J. Appl. Phys. **94**, 6346 (2003).
[32] J. M. Sanchez, F. Ducastelle, and D. Gratias, Physica A **128**, 334 (1984).
[33] L. Bellaiche, S.-H. Wei, and A. Zunger, Phys. Rev. B **54**, 17568 (1996).
[34] P. R. C. Kent and A. Zunger, Phys. Rev. B **64**, 115208 (2001).
[35] K. Kim, W. R. L. Lambrecht, and B. Segall, Phys. Rev. B **53**, 16310 (1996).
[36] A. F. Wright, J. Appl. Phys. **82**, 2833 (1997).
[37] J. L. Martins and A. Zunger, Phys. Rev. B **30**, 6217 (1984).
[38] A. Polian, M. Grimsditch, and I. Grzegory, J. Appl. Phys. **79**, 3343 (1996).
[39] M. van Schilfgaarde, A. Sher, and A.-B. Chen, J. Cryst. Growth **178**, 8 (1997).
[40] K. Kim, P. R. C. Kent, A. Zunger, and C. B. Geller, Phys. Rev. B **66**, 045208 (2002).
[41] P. E. Blöchl, Phys. Rev. B **50**, 17953 (1994).
[42] G. Kresse and J. Furthmüller, Comput. Mater. Sci. **6**, 15 (1996); G. Kresse and D. Joubert, Phys. Rev. B **59**, 1758 (1999).
[43] S. Froyen, Phys. Rev. B **39**, 3168 (1989).
[44] H. J. Monkhorst and J. D. Pack, Phys. Rev. B **13**, 5188 (1976).
[45] A. Zunger, S.-H. Wei, L. G. Ferreira, and J. E. Bernard, Phys. Rev. Lett. **65**, 353 (1990).
[46] S.-H. Wei, L. G. Ferreira, J. E. Bernard, and A. Zunger, Phys. Rev. B **42**, 9622 (1990).
[47] S.-H. Wei, L. G. Ferreira, and A. Zunger, Phys. Rev. B **41**, 8240 (1990).
[48] Z. W. Lu, D. B. Laks, S.-H. Wei, and A. Zunger, Phys. Rev. B **50**, 6642 (1994).
[49] S. Chen, X. G. Gong, and S.-H. Wei, Phys. Rev. B **77**, 073305 (2008).
[50] A. A. Mbaye, D. M. Wood, and A. Zunger, Phys. Rev. B **37**, 3008 (1988).
[51] J. Z. Liu, G. Trimarchi, and A. Zunger, Phys. Rev. Lett. **99**, 145501 (2007).
[52] At each composition, we calculated the standard deviation among the 10 random realizations. The average of the standard deviations taken over all compositions is 0.7 meV/cation for GaInN, 0.3 meV/cation for GaInP, 1.2 meV/cation for InNP, and 1.6 meV/cation for GaNP.
[53] C. K. Gan, Y. P. Feng, and D. J. Srolovitz, Phys. Rev. B **73**, 235214 (2006).
[54] J. A. Purton, M. Yu. Lavrentiev, and N. L. Allan, J. Mater. Chem. **15**, 785 (2005).
[55] C. Caetano, L. K. Teles, M. Marques, A. Dal Pino, Jr., and L. G. Ferreira, Phys. Rev. B **74**, 045215 (2006).
[56] L. K. Teles, J. Furthmüller, L. M. R. Scolfaro, J. R. Leite, and F. Bechstedt, Phys. Rev. B **62**, 2475 (2000).
[57] M. Ferhat and F. Bechstedt, Phys. Rev. B **65**, 075213 (2002).
[58] S. Y. Karpov, N. I. Podolskaya, I. A. Zhmakin, and A. I. Zhmakin, Phys. Rev. B **70**, 235203 (2004).
[59] D. A. Porter and K. E. Easterling, *Phase Transformations in Metals and Alloys*, 2nd ed. (CRC, Boca Raton, FL, 1991).
[60] A. Tabata, J. R. Leite, A. P. Lima, E. Silveira, V. Lemos, T. Frey, D. J. As, D. Schikora, and K. Lischka, Appl. Phys. Lett. **75**, 1095 (1999).
[61] E. Silveira, A. Tabata, J. R. Leite, R. Trentin, V. Lemos, T. Frey, D. J. As, D. Schikora, and K. Lischka, Appl. Phys. Lett. **75**, 3602 (1999).
[62] V. Lemos, E. Silveira, J. R. Leite, A. Tabata, R. Trentin, L. M. R. Scolfaro, T. Frey, D. J. As, D. Schikora, and K. Lischka, Phys. Rev. Lett. **84**, 3666 (2000).
[63] R. Singh, D. Doppalapudi, T. D. Moustakas, and L. T. Romano, Appl. Phys. Lett. **70**, 1089 (1997).
[64] D. Doppalapudi, S. N. Basu, K. F. Ludwig, Jr., and T. D. Moustakas, J. Appl. Phys. **84**, 1389 (1998).

[65] T. P. Bartel, P. Specht, J. C. Ho, and C. Kisielowski, Philos. Mag. **87**, 1983 (2007).
[66] Z. Liliental-Weber, D. N. Zakharov, K. M. Yu, J. W. Ager III, W. Walukiewicz, E. E. Haller, H. Lu, and W. J. Schaff, Physica B (Amsterdam) **376-377**, 468 (2006).
[67] S. B. Zhang and A. Zunger, Appl. Phys. Lett. **71**, 677 (1997).
[68] W. G. Bi and C. W. Tu, Appl. Phys. Lett. **69**, 3710 (1996).
[69] J. A. Gupta, W. R. McKinnon, J. Noad, D. Coulas, R. L. Williams, R. Driad, and S. P. McAlister, J. Cryst. Growth **231**, 48 (2001).